1   **Loss of midbrain dopamine neurons and altered apomorphine EEG effects in the 5xFAD**

2   **mouse model of Alzheimer's disease**

3   Vasily Vorobyov[a], Boris Bakharev[a], Natalia Medvinskaya[a], Inna Nesterova[a], Alexander

4   Samokhin[a], Alexander Deev[b], Olga Tatarnikova[a], Aleksey A Ustyugov[c], Frank Sengpiel[d], Natalia

5   Bobkova[a]

6

7   [a]*Institute of Cell Biophysics, Russian Academy of Sciences, 142290 Pushchino, Moscow Region,*

8   *Russian Federation*

9   [b]*Institute of Theoretical and Experimental Biophysics, Russian Academy of Sciences, 142290*

10   *Pushchino, Moscow Region, Russian Federation*

11   [c]*Institute of Physiologically Active Compounds, Russian Academy of Sciences, 142432,*

12   *Chernogolovka, Moscow Region, Russian Federation*

13   [d]*School of Biosciences and Neuroscience & Mental Health Research Institute, Cardiff University,*

14   *Museum Avenue, Cardiff CF10 3AX, UK*

15

16   **Running head:** *EEG in 5xFAD mice*

17

18

19   **Corresponding author:**

20   Dr. V. Vorobyov, PhD

21   Institute of Cell Biophysics

22   Pushchino, 142290

23   Russian Federation

24   Tel: 007-4967-739-223

25   Fax: 007-4967-330-509

26   E-mail: vorobyovv2@gmail.com

27

Abstract

Cognitive malfunction, synaptic dysfunction, and disconnections in neural networks are core deficits in Alzheimer's disease (AD). 5xFAD mice, a transgenic model of AD, are characterised by an enhanced level of amyloid-*beta* and abnormal neurotransmission. The dopaminergic (DA) system has been shown to be involved in amyloid-*beta* transformations and neuronal plasticity; however, its role in functional network changes in familial AD still remains unclear. In 5xFAD and non-transgenic freely moving mice, electroencephalograms (EEGs) were simultaneously recorded from the secondary motor cortex (MC), superficial layers of the hippocampal CA1 area (HPC), substantia nigra (SN), and ventral tegmental area (VTA). EEGs and their frequency spectra were analysed before and after systemic injection of a DA receptor agonist, apomorphine (APO). In the baseline EEG from MC and HPC of 5xFAD mice, *delta* and *alpha* oscillations were enhanced and *beta* activity was attenuated, compared to control mice. In VTA and SN of 5xFAD mice, *delta-theta* activity was decreased and *beta* oscillations dominated. In control mice, APO suppressed *delta* activity in VTA to a higher extent than in MC, whereas in 5xFAD mice, this difference was eliminated due to attenuation of the *delta* suppression in VTA. APO increased *beta* activity in MC of mice from both groups while significant *beta* suppression was observed in VTA of 5xFAD mice. These mice were characterized by significant decrease of tyrosine hydroxylase immunopositive cells in both VTA and SN and of DA transporter in MC and hippocampal dentate gyrus. We suggest that the EEG modifications observed in 5xFAD mice are associated with alterations in dopaminergic transmission, resulting in adaptive changes in the cerebral networks in the course of familial AD development.

Key words: secondary motor cortex; hippocampus; ventral tegmental area; substantia nigra; DAT; electroencephalogram; frequency spectrum

1. Introduction

Alzheimer's disease (AD), characterized by neurodegeneration, pathological formation of extracellular amyloid plaques and intraneuronal aggregation of hyperphosphorylated tau into neurofibrillary tangles in the brain, is associated with a gradual decline of cognitive abilities (for review, see [1]). Synaptic dysfunction and an imbalance between coordinated activities of different brain structures is hypothesized to be the main cause of abnormal functioning of the diseased brain [2 - 5]. Cognitive decline in AD is thought to be associated with alterations in synaptic transmission and thus in neuronal network function that is accompanied by modification of oscillations in the affected circuits [6, 7]. Superimposed extracellular fields arising from synaptic transmembrane currents of neurons involved in the circuits are supposed to form the electroencephalogram (EEG) [8] whose frequency composition has been shown to be associated with cognitive abilities of AD patients [9]. Substantial changes in the interhemispheric asymmetry in cortical EEG frequency spectra, demonstrated in AD patients [10], are in line with the well-known role of interhemispheric transfer for effective learning and memory [11]. Furthermore, changes in EEG recorded from the frontal cortex and/or the hippocampus, key brain areas in learning and memory processing, have been shown in an amyloid rat model of AD [12] and in numerous transgenic mouse models of AD [13 - 19].

Among transgenic mice, the 5xFAD line is distinguished by expressing multiple familial AD (FAD) mutations that additively increase amyloid-$beta_{42}$ (Aβ_{42}) production, the main hallmark in AD, and by causing dissociation between cortical and hippocampal synaptic plasticity [20], changes in cortical excitability and hippocampal rhythmicity, and defects in cholinergic transmission [18]. 5xFAD mice have been shown to exhibit intraneuronal Aβ accumulation at 1.5 months, Aβ deposition at 2 months, and memory deficits at 4 months of age [21] that are accompanied by defects in synaptic vesicle dynamics and neurotransmitter release [22]. Despite a significant Aβ accumulation, the overall numbers of neurons in the frontal cortex and hippocampus in 5xFAD mice have been shown to equal those in age-matched controls, with the exception of a neuronal loss in cortical layer 5 [23]. Interestingly, before this specific structural dystrophy, synaptic deficits in layer 5 neurons were observed [24]. Thus, a deeper insight into the activities of different brain networks and their changes in the 5xFAD mice promises to aid effective analysis of the AD pathogenesis [18].

In a number of recent studies on AD transgenic mice (and 5xFAD, in particular), substantial attention has been paid to neuronal networks within/between the cortex and the hippocampus [12, 17 - 20, 25, 26]. Furthermore, the role of cholinergic, monoaminergic, and GABA-ergic transmission in the functioning of these networks has been shown [18, 25, 27]. In our previous study on an amyloid AD model, involvement of the dopaminergic (DA) system in the cortex-hippocampus EEG interplay has been revealed [12]. However, we are still lacking detailed information how this system is affected in the AD transgenic mice. This needs to be clarified

90   given data demonstrating a role of the DA system in both neuronal plasticity and amyloid-*beta*

91   transformations in AD [28 - 30].

92   In this study on 5xFAD and non-transgenic (control) adult mice, we recorded EEGs from the

93   secondary motor cortex, dorsal hippocampus, and from two DA-producing areas, the substantia

94   nigra and ventral tegmental area, before and after systemic injection of a DA receptor agonist,

95   apomorphine. Significant differences between 5xFAD and control mice were revealed in

96   frequency spectra of both baseline and APO-evoked EEG activities in and between the brain

97   areas.

98

99   **2. Materials and Methods**

100   Twelve six-month old male transgenic (Tg) mice with five familial AD mutations (5xFAD mice,

101   B6SJL-Tg(APPSwFlLon,PSEN1*M146L*L286V)6799Vas/J) were maintained on the C57BL/6J

102   genetic background and fifteen non-transgenic (nTg, wild type control) littermates were used in

103   this study. The 5xFAD mice were originally obtained from the Center for Collective Use of the

104   Institute of Physiologically Active Compounds RAS (Chernogolovka, Russian Federation). Up to

105   the age of five months, the mice were housed in groups of five per cage, while, thereafter, each

106   of them was kept for 1.5 months in an individual cage. Mice were housed in a standard

107   environment (12-h light/dark cycle, 22-25°C room temperature, 50-55% relative humidity) with

108   food and water *ad libitum*. The procedures were carried out in accordance with the "Guidelines

109   for accommodation and care of animals. Species-specific provisions for laboratory rodents and

110   rabbits" (GOST 33216-2014) and in compliance with the principles enunciated in the Directive

111   2010/63/EU on the protection of animals used for scientific purposes, and approved by the local

112   Institute Ethics Review Committee. All efforts were made to minimize both the number of the

113   animals and their suffering.

114   All mice were genotyped using PCR analysis of DNA obtained from the ear/tail biopsy,

115   followed by separation of the reaction products in the agarose gel. Mice with a transgene

116   cassette in the genome were combined into Tg group, whereas those with lacking transgene

117   were placed into nTg group. Post-mortem verification of the amyloid plaques in the brain slices

118   (Suppl. 1), stained with thioflavin-S [32], revealed this AD hallmark in all mice from the Tg group.

119   *2.1. Electrodes implantation and EEG recording*

120   After one month of adaptation to the individual cage, each of six 5xFAD mice (29.7 ± 0.5 g)

121   and nine nTg mice (33.0 ± 1.1 g) was anesthetized with subcutaneous (s.c.) injection of a

122   combination of dissolved tiletamine/zolazepam (Zoletil®, Virbac, France) and xylazine solution

123   (Rometar®, Bioveta, Czech Republic) at doses of 25 mg/kg and 2.5 mg/kg, respectively. Four

124   recording electrodes were implanted into the left secondary motor cortex (MC; AP: +1.9, ML: -0.4,

125   DV: -2.0), over the left dorsal hippocampus (HPC; AP: -2.8, ML: -2.7, DV: -1.7), into the left

126 ventral tegmental area (VTA; AP: -3.1, ML: -0.4, DV: -4.5), and into the right substantia nigra (SN;
127 AP: -3.2, ML: +1.3, DV: -4.3) [33] (DV was measured from the skull surface). Within areas
128 analyzed in this study, the opposite hemisphere for SN was chosen, firstly, because of its
129 proximity to VTA which meant we could not exclude possible mutual damage during electrode
130 implantation in the same hemisphere. Secondly, it is well known that the contralateral SN is the
131 dominant source of DA in the opposite (here: left) hemisphere. Custom made electrodes were
132 constructed from two varnish-insulated nichrom wires (100-µm diameter) glued together (3M
133 Vetbond™ Tissue Adhesive, MN, USA) with tips free from insulation for 100 µm. Thus, prepared
134 electrodes were sufficiently inflexible, and had higher effective surface/volume ratio than a mono-
135 wire electrode of 200-µm diameter. The reference and ground electrodes (stainless steel wire, 0.4
136 mm in diameter) were placed symmetrically into the caudal cavities behind the cerebrum (AP: -
137 5.3, ML: ±1.8, DV: -0.5). All electrodes were positioned using a computerized 3D stereotaxic
138 StereoDrive (Neurostar, Germany), fixed to the skull with dental cement and soldered to a dual
139 row female connector (Sullins Connector Solutions, CA, USA). Both nichrom wires of the deep
140 electrode were soldered to one of the connector's pins. After electrode implantation, animals were
141 housed individually. *Post-mortem* verification of the electrode tip location included several steps:
142 an anodal current (80-100 µA, 1 s) coagulation of the adjacent tissue, extirpation of the brain and
143 fixation of the cerebrum in 4% paraformaldehyde. The brain was cut in 30-µm sections using a
144 freezing microtome (Reicher, Austria). Coronal sections were examined to specify the electrode
145 tip locations; EEG recordings from those, which did not meet placement criteria, were excluded
146 from further analysis. Effective electrode targeting of the chosen brain areas was based on the
147 use of the stereotaxic manipulator and on precise measurement of bregma and lambda
148 coordinates. This high-tech manipulator allows the drilling of the holes for the electrodes exactly
149 in the selected points on the skull. Precise estimations of an individual's bregma-lambda distance
150 provides the correction of the coordinates for the brain areas, taking into account that the value
151 used for preparation of the stereotaxic atlas [33] was equal to 4.2±0.25 mm. In several cases,
152 when the electrolytic marker was relatively enlarged, the electrode tip position was assigned to
153 the point where the effect of electrolysis within the coagulated area was maximal. The frozen
154 slices with the most effective electrode position were Nissl stained with cresyl violet acetate [34],
155 magnified (Nikon Eclipse E200 microscope, Japan), digitized (DXM1200 camera, Japan), and
156 used for illustration in combination with corresponding images of the mouse brain atlas [31]
157 (Suppl. 2).
158 Three days after electrode implantation, each mouse was adapted for four days (1 h/day) to an
159 experimental cage (Perspex, 15x17x20 cm) located in an electrically shielded chamber and to a
160 cable (five 36-gauge wires, Plexon Inc, Texas, USA) plugged in a digital Neuro-MEP amplifier
161 (Neurosoft Ltd, Ivanovo, Russian Federation). On day 8, a baseline EEG was recorded for 60
162 min, starting 20 min after placing the animal into the box. EEG recordings were continued for 120

163 minutes after s.c. injection either saline (control) or, on the next day, apomorphine (APO, Sigma,

164 Milan, Italy), at a dose of 1.0 mg/kg. To minimize the effect of oxidation only freshly dissolved

165 APO was used. All experiments were performed from 9 am to 6 pm in daylight combined with an

166 artificial light source keeping illumination at a relatively stable level.

167 *2.2. Computation of EEG frequency spectra*

168   Monopolar EEG signals measured between the active and reference electrodes were

169 amplified, filtered (0.1-35 Hz) and sampled (1 kHz) on-line using the amplifier and kept in memory

170 of an operational computer for further analysis. The frequency spectra of successive 12-sec EEG

171 epochs were studied using a modified version of period-amplitude analysis [35], which, in

172 contrary to the Fourier transform, was not affected by well-known non-stationary nature of the

173 EEG signals. The *absolute values* of the *half-wave* amplitudes with periods/frequencies in each of

174 selected narrow EEG frequency subbands were summed followed by their normalization to the

175 summarized values. In this study, twenty subbands in the 0.48 - 26.25 Hz range were analyzed:

176 0.48 - 0.53 (**0.5**), 0.87 - 0.97 (**0.9**), 1.29 - 1.43 (**1.4**), 1.74 - 1.92 (**1.8**), 2.21 - 2.44 (**2.3**), 2.71 - 3.0

177 (**2.9**), 3.25 - 3.59 (**3.4**), 3.82 - 4.22 (**4.0**), 4.44 - 4.91 (**4.7**), 5.12 – 5.66 (**5.4**), 5.86 - 6.48 (**6.2**), 6.68

178 - 7.38 (**7.0**), 7.59 - 8.39 (**8.0**), 8.63 - 9.54 (**9.1**), 9.83 – 10.86 (**10.3**), 11.25 - 12.43 (**11.8**), 12.98 -

179 14.35 (**13.7**), 15.21 - 16.82 (**16.0**), 18.36 - 20.3 (**19.3**), 23.75 - 26.25 (**25.0**). The subbands are

180 marked in figures by their centre (mean) frequency values (see in brackets, above). The terms

181 "lower" and "higher" in "classical" EEG bands *delta* (0.5 - 3.6 Hz), *theta* (3.8 - 8.4 Hz), *alpha* (8.6 -

182 12.4 Hz), and *beta* (12.9 - 26.2), are used below to differentiate corresponding frequency

183 subbands of each band relative to its centre frequency (for more details, see [12]).

184   The frequency spectra of 12-sec EEG epochs were averaged for every successive 10-min

185 interval for each mouse and for all of them separately from nTg and Tg groups. Relative

186 differences in the averaged EEG spectra, obtained in the experiments with saline (day 1) and

187 APO (day 2) in each group, were estimated as (APO - Saline) / Saline, in percentages, which

188 providing the evaluation of APO effects in nTg and Tg groups.

189 *2.3. Immunohistochemical techniques*

190   In additional groups of 5xFAD and nTg mice (n = 6 in each group), the animals were deeply

191 anaesthetized with ether and transcardially perfused consecutively with ice-cold saline and 4%

192 paraformaldehyde in phosphate-buffered solution (PBS). Afterwards, the brains were promptly

193 removed from the cranium and kept in the paraformaldehyde/PBS solution at 4°C for further

194 histochemical analysis. For each animal, coronal brain sections (20-μm thick) at the level of VTA

195 and SN were prepared using a freezing microtome (Reicher, Austria) and stored at -20°C in a

196 cryoprotective solution (30% glycerol, 30% ethylene glycol in 0.05M PBS). To evaluate tyrosine

197 hydroxylase (TH) immunoreactive cell populations in VTA and SN the slices were washed with

198 water and subsequently incubated overnight with rabbit polyclonal anti-TH antibodies (1:500,

199 Chemicon, Woburn, MA, USA). Afterwards, they were incubated for one hour at room

200 temperature with biotinylated goat secondary antibodies against rabbit's immunoglobulin (1:200,

201 Abcam, UK) and with avidin-biotin-peroxidase complex (1:400, Sigma, USA). Peroxide content in

202 the slices was measured after their incubation in a composition of 3,3'-diaminobenzidine-

203 tetrahydrochloride (DAB; Sigma, St. Louis, USA) and H_2O_2 (at 0.05% and 0.02%, respectively) for

204 3-3.5 min at 20°C, followed by washing with PBS and fixation on gelatine-coated glass slides.

205 Images of the brain slices were magnified (20x) and digitized (Nikon Eclipse E200 microscope

206 and DXM1200 camera, respectively, Japan) for the count of the DA-producing neurons in the

207 VTA and SN borders outlined using the atlas of TH-positive cells distribution [36]. The number of

208 tyrosine hydroxylase immunopositive (TH+) cells was manually counted inside of symmetrical

209 VTA and SN contours on each slide. Within thirty consecutive sections at the level of VTA and

210 SN, five of them (every sixth one) were used for this analysis. Thus, the total statistics data were

211 based on 2 x 5 x 6 = 60 contours of VTA or SN, meaning two symmetrical areas on one slide, five

212 slides, and six animals, respectively. Averaged data obtained on ten contours per mouse were

213 used in the final statistics on all animals.

214 The brain sections at the level of MC and HPC from the same mice were washed in PBS with

215 Triton X100 and treated with H_2O_2 to inactivate endogenous peroxidase. They were consequently

216 incubated with rabbit polyclonal anti-dopamine transporter antibody (MilliporeSigma, USA), with

217 Biotin-conjugated goat secondary antibody (MilliporeSigma, USA), and, finally, with ExtraAvidin-

218 Peroxidase (Sigma, USA), all diluted 1:300. After staining with DAB (Sigma, USA) and mounting

219 on the pre-coated glass slides (Superfrost-plus Menzel, Germany), the slices were cover-slipped

220 (Coverquick, Labonord, France) and analyzed at magnification of 20x using the microscope

221 (Nicon E200, Japan). Dopamine transporter (DAT) levels were assessed symmetrically in both

222 MC and HPC (the dentate gyrus, CA1-CA2, and CA3-CA4 areas) in five coronal sections (every

223 sixth of thirty ones) per animal. Digitized images of 0.25 mm^2 in the target brain areas were

224 analyzed by use of the Picture Analyzer Software, ImageJ, which estimated the DAB staining

225 area. Averaged data obtained in ten 0.55 mm x 0.45 mm frames (0.25 mm^2) per mouse were

226 used in final statistics on all six animals.

227

228 *2.4. Statistics*

229 Differences in the averaged EEG spectra were evaluated by a two-tailed non-parametric

230 Mann-Whitney U-test for individual frequency subbands, and by ANOVA for repeated measures

231 when progression of EEG effects in the frequency ranges was analyzed either separately in

232 different brain areas (one-way ANOVA) or between them (2-way ANOVA). Immunohistochemical

233 data were analysed by a two-tailed non-parametric Mann-Whitney U-test with Bonferroni

234 correction. The group data were expressed as the means ± SEM; differences were considered

7

235   significant at p < 0.05. For ANOVA and U-test analyses, STATISTICA 10 (StatSoft, Inc., Tulsa,

236   OK, USA) was used, whereas power and effect size were calculated by use of G*Power 3.1.9.4

237   (www.psycho.uni-duesseldorf.de/abteilungen/aap/gpower3). At the effect size of 0.75 - 0.9 and

238   power of 0.8, G*Power showed that the sample sizes chosen for nTg and Tg groups (9 and 6

239   mice, respectively) were reasonable for our EEG study (see below).

240

241   **3. Results**

242   *3.1. Baseline EEG from different brain areas*

243   During baseline EEG recordings, both non-transgenic (nTg) and transgenic (Tg) 5xFAD mice

244   were behaviorally active and characterized by intensive exploration of the experimental box that

245   was very rarely (1-2/60 min) interrupted by short (< 60 sec) sleep-like bouts.

246   Baseline EEGs in freely moving and behaviourally active nTg and Tg (5xFAD) mice (Fig. 1 A

247   and B, respectively) were characterized in MC and HPC by patterns of relatively slow (5 - 7 Hz)

248   and very fast (14 - 25 Hz) oscillations. In the EEG from VTA, these patterns were also observed

249   in Tg mouse, whereas powerful slow waves of 3 - 7 Hz were characteristic for nTg mouse. In the

250   EEG from SN in nTg mouse, oscillations of 6 - 12 Hz predominated. The EEG patterns from MC

251   and HPC were represented in their frequency spectra by peaks in *theta* and *beta* bands (Fig. 1,

252   C, D). EEG spectra from VTA and SN in nTg mouse were characterized by wide peaks in the

253   ranges of *theta* and *theta-alpha*, respectively, whereas, in Tg mouse, the peaks were found in the

254   *lower theta and higher alpha-beta* (Fig. 1, E, F). These differences between the groups were

255   stable in EEG spectra averaged over consecutive 10-min intervals and, thus, evidently observed

256   in the spectral profiles that characterised the whole (60-min) baseline period (Fig. 2).

257   In 5xFAD mice, EEG activity in MC was enhanced during this period in both *delta* and *alpha*

258   bands and suppressed in *beta* band, compared to those in nTg mice (Fig. 2, A; 2-way ANOVA for

259   15 samples x 6 repeats: $F_{1,78} > 15$, $p < 0.001$, for all bands). In HPC, the EEG differences in *delta*

260   and *beta* bands *between the groups* were similar to those in MC (Fig. 2, B; 2-way ANOVA for 15

261   samples x 6 repeats: $F_{1,78} > 28$, $p < 0.001$, for both bands). In VTA of 5xFAD mice, relatively slow

262   oscillations in *delta - theta* range were attenuated, whereas *beta* activity was enhanced,

263   compared to those in nTg mice (Fig. 2, C; 2-way ANOVA for 15 samples x 6 repeats: $F_{1,78} > 34$, p

264   < 0.001, for both frequency ranges). In SN (Fig. 2, D), significant differences between 5xFAD and

265   nTg mice were observed in the same frequency ranges (2-way ANOVA for 15 samples x 6

266   repeats: $F_{1,78} > 24$, $p < 0.001$, for both ranges), however, the differences were evidently less than

267   in VTA (c.f., Fig. 2, C and D, grey bars). All mentioned above differences were characterised by

268   reasonable power and effect size measures (see Suppl. 3).

269   Averaged EEG frequency spectra in MC were identical to those in HPC in both groups of mice

270   (Fig. 3, A). EEG differences between VTA and SN (Fig. 3, B), enhanced in *delta-theta* range and

271   reduced in *beta* band in nTg mice, were diminished in 5xFAD mice (2-way ANOVA for 15

8

272   samples x 6 repeats: $F_{1,78}$ = 8.8, p < 0.01 and $F_{1,78}$ = 6.3, p < 0.05, for both frequency ranges). In

273   nTg mice, EEG differences between VTA and MC (Fig. 3, C, dotted line), increased in *delta-alpha*

274   range and decreased in *beta* band, were reduced in 5xFAD mice (Fig. 3, C, solid line) (2-way

275   ANOVA for 15 samples x 6 repeats: $F_{1,78}$ > 270, p < 0.001, for both frequency ranges). The

276   profiles of relative differences between EEG spectra in SN and MC in nTg mice (Fig. 3, D, dotted

277   line) were similar to those observed between VTA and MC. In 5xFAD mice, the EEG spectral

278   differences between SN and MC (Fig. 3, D, solid line) were significantly diminished in *delta-alpha*

279   range and in *beta* band (2-way ANOVA for 15 samples x 6 repeats: $F_{1,78}$ > 40, p < 0.001, for

280   both). All mentioned above differences were characterised by reasonable power and effect size

281   measures (see Suppl. 4).

282

283   *3.2. Apomorphine effects*

284   After APO injection, behavioral reactions of both Tg and nTg mice were stereotyped: short-

285   lasting freezing (1.5-2 min), followed by uninterrupted licking of the lower sides of the box that

286   was accompanied by raising the tail. The behavioral response was comparable between Tg and

287   nTg mice. Sleep-like bouts were very rare and short, and occurred at variable times.

288   In several pilot/supporting experiments on four nTg and three Tg mice, variations in EEG

289   spectra after saline injections in two consecutive days were evaluated. In spite of visible scattered

290   fluctuations in the EEG spectra averaged over consecutive 10-min intervals, no significant

291   regularities in the frequency-time domain were observed (see Suppl. 5). Given these preliminarily

292   obtained findings and obvious advantage of the experimenting on the same mouse, the sequence

293   of saline and APO injections in day 1 and day 2, respectively, was chosen as preferable.

294   APO produced significant changes in *cortical* EEG activities in *delta* and *beta* bands (Fig. 4, A

295   and B, respectively) compared to those observed after saline injection both in nTg mice (1-way

296   ANOVA for 9 samples x 12 repeats: $F_{11,96}$ = 3.8, p < 0.001 and $F_{11,95}$ = 2.6, p < 0.05 for *delta* and

297   *beta* bands, respectively) and in 5xFAD mice (1-way ANOVA for 6 samples x 12 repeats: $F_{11,60}$ =

298   3.3, p < 0.01 and $F_{11,60}$ = 3.0, p < 0.01, for *delta* and *beta* bands, respectively). APO-induced

299   *delta* suppression and *beta* enhancement in the cortex were observed for 50 min after injection

300   and both were more powerfully expressed in 5xFAD mice, compared to those in nTg mice (2-way

301   ANOVA for 15 samples x 5 repeats: $F_{1,65}$ = 5.4, p < 0.05 and $F_{1,\,65}$ = 9.8, p < 0.01, for *delta* and

302   *beta* bands, respectively). Similar APO effects revealed in *hippocampal* EEG (Fig. 4, C, D)

303   evidently dominated for the whole 120-min period in 5xFAD mice over those in nTg mice in both

304   *delta* and *beta* bands (2-way ANOVA for 15 samples x 12 repeats: $F_{1,156}$ = 15.2, p < 0.001 and

305    $F_{1,155}$ = 24.5, p < 0.001, respectively). In EEG from *VTA*, APO suppressed *delta* activity for 50

306   minutes to a similar extent in both groups (Fig. 4, E; 2-way ANOVA for 15 samples x 12 repeats:

307    $F_{1,156}$ = 0.8, p = 0.4). In contrast, *beta* activity was significantly enhanced in 5xFAD mice

308   compared to that in nTg mice (Fig. 4, F; 2-way ANOVA for 15 samples x 12 repeats: $F_{1,156}$ = 11.0,

309   p < 0.01). The profiles of APO effect in *SN* (Fig. 4, G, H) were similar to those observed in VTA.

310   The main differences between APO effects in nTg and Tg mice were predominantly observed for

311   50 minutes after APO injection and characterised by reasonable power and effect size measures

312   (see Suppl. 6).

313   After APO injection, the main interregional differences between the groups were revealed in

314   MC and VTA (Fig. 5). In nTg mice, APO suppressed *delta* activity in VTA for 50 min after injection

315   to significantly higher extent than in MC (Fig. 5, A). In 5xFAD mice (Fig. 5, B), this difference was

316   eliminated predominantly due to its enhancement in VTA (c.f., Fig. 5, A and B, black lines; 2-way

317   ANOVA for 12 samples x 12 repeats: $F_{1,156} = 14.4$, $p < 0.001$). After APO injection, *beta* activity in

318   MC was increased for 50 minutes in both nTg and 5xFAD mice (Fig. 5, C and D, respectively,

319   grey lines). In nTg mice, APO produced phasic response in *beta* activity in VTA that was tended

320   to be lower relative to that in MC (Fig. 5, C, black and grey lines, respectively). In 5xFAD mice,

321   *beta* activity in VTA was significantly suppressed by APO, compared to that in MC (Fig. 5, D; 2-

322   way ANOVA for 12 samples x 12 repeats: $F_{1,156} = 10.7$, $p < 0.01$). The differences in APO effects

323   revealed in EEG from VTA and MC in nTg and Tg mice (Fig. 5, A and D, respectively) were

324   characterised by reasonable power and effect size measures (see Suppl. 7).

325

326   *3.3. DA cells and dopamine transporter (DAT) distribution*

327   To investigate the impact of possible differences in the DA system in Tg and nTg mice on their

328   EEG spectra, we stained brain sections with antibodies against TH or DAT at the levels of VTA-

329   SN or MC-HPC areas, respectively (see Materials and Methods). The approaches revealed a

330   significant decrease of both TH-positive (TH+) cells in the DA-producing areas and DAT vesicle

331   density in the forebrain areas in 5xFAD mice (Fig. 6, A, C and B, D, respectively).

332

333   **4. Discussion**

334   In this study, we have shown significant differences between transgenic, 5xFAD, and non-

335   transgenic (nTg), control, mice in *baseline* and *apomorphine-modified EEGs* recorded from

336   different brain areas: secondary motor cortex (MC), hippocampus (HPC), ventral tegmental area

337   (VTA), and substantia nigra (SN).

338   *Baseline EEG*

339   In baseline EEG from MC and HPC in 5xFAD mice, *delta* and *alpha* oscillations were more

340   powerfully expressed than in nTg mice whereas those in *beta* band were suppressed (Fig. 2, A,

341   B). The increase of *delta* waves in the EEGs recorded from MC and HPC in 5xFAD mice seems

342   to be typical for transgenic murine AD models, as slower EEG activity has been shown in 5xFAD,

343   TgCRND8, and APP single mutant mice [13, 16, 18]. The EEG alterations in transgenic mice are

344   thought to be linked to the Aβ accumulation and plaque formation [17, 19]. However, EEG

345   modifications associated with the *theta-gamma* coupling, in particular, have been shown in

346 transgenic mice to precede the excessive Aβ production and other AD features [16]. In adult

347 5xFAD mice, which have been shown to be characterized by typical AD indices (see, e.g., [21]),

348 we demonstrate the slowing down of cortical and hippocampal oscillations in both *theta-delta* and

349 *beta-alpha* ranges (Fig. 2, A, B). These effects seem to be associated with a significant

350 suppression of DAT (Fig. 6, B, D) that might be expected to be associated with increase in DA in

351 the synaptic cleft [37], which hypothetically is able to compensate, at least in part, for the loss of

352 DA-producing neurones in VTA and SN (Fig. 6, A, C). The low level of DA receptor activation has

353 been shown to be accompanied by EEG sleep features in the cortex [38]. Indeed, in 5xFAD mice,

354 we observe a significant amplification of both *delta* and *alpha* oscillations in MC (Fig. 2, A), a

355 hallmark of so-called "non-REM" sleep [39]. Transformation of *theta* and *beta* oscillations, which

356 dominated in nTg mice, into a *delta* and *alpha* activities in 5xFAD mice suggesting the oscillatory

357 circuits affected by excessive Aβ in transgenic mice have a potential for adaptive remodelling in

358 response to the neurotoxicity of soluble Aβ [40], intraneuronal Aβ$_{42}$-induced neurodegeneration

359 and amyloid plaque formation, which are typical for 5xFAD mice [21]. Thus, further discovery of

360 the mechanisms underlying reorganizing of disrupted neuronal circuits, involved, in particular, in

361 sleep initiation might be useful for the development of a new therapeutic approach.

362 In EEG from VTA and SN in 5xFAD mice, averaged amplitudes of *delta-theta* waves were

363 significantly decreased whereas those of beta rhythms were increased (Fig. 2, C, D). These

364 frequency ranges coincide with those that characterise tonic (*delta-theta*) and so-called "bursting"

365 (*beta*) neuronal activities in the DA-producing areas [41, 42]. Given these and an involvement of

366 transmembrane currents in the origin of the EEG [8], the spectral differences in EEG from VTA

367 and SN may be interpreted as a weakening of tonic spiking and strengthening of phasic bursting

368 activity of DA neurones in 5xFAD mice. This is in line with an about four-fold higher rate of

369 bursting patterns revealed in rats after long-term 6-hydroxydopamine lesions of DA neurons in

370 SN [43]. The bias in profiles of VTA and SN neuronal activities is supposedly linked with DA cell

371 loss in 5xFAD mice (Fig. 6, A, C). Evident correlation between the extent of DA cell loss in VTA

372 (63%) and SN (48%), and *beta* activity increase in EEG from these areas (37% and 20%,

373 respectively) in 5xFAD mice is in line with this suggestion (Fig. 2, C, D, grey bars in *beta* band).

374 Partial DA cell loss is expected to invoke compensatory feed-back and feed-forward mechanisms

375 [44]. Indeed, MC activation has been shown to initiate bursts in VTA neurons [45] effectively

376 stimulating DA release in the cortex [46, 47]. This seems to be a vivid manifestation of a

377 compensatory function of the MC-VTA networks in 5xFAD mice, which are characterized by

378 depleted DAT in MC (Fig. 6, B, D) that is well known to initiate compensatory modifications in DA

379 synapses [48].

380 In our study, the functioning of networks formed by different brain areas was evaluated

381 through the relations between their EEG frequency spectra (Fig. 2). In mice from both groups, the

382 relative spectral profiles of EEG from HPC and MC were flat (Fig. 3, A). Thus, the slowing of

383   EEGs from these areas in Tg mice (Fig. 2, A, B, grey bars) seems to be associated with

384   synchronization of cortical and hippocampal oscillations that, in turn, may be correlated with the

385   DAT level reduction observed in MC in 5xFAD mice (Fig. 6, B, D). Indeed, DA infusion into MC

386   has been shown to produce a significant enhancement of EEG synchronization and/or coherence

387   in MC and HPC [49]. Together, these suggest that DA transmission in the MC-HPC neuronal

388   circuits in 5xFAD mice is unchanged.

389   *In control mice*, VTA recordings were characterized by increased *higher delta*-lower *theta* and

390   decreased *lower alpha-beta* ranges (Fig. 2, C, grey line), that may be interpreted as a

391   predominance of tonic discharges in VTA neurons and "bursting" activity in SN (see above). This

392   specificity of DA-containing areas, revealed in their EEG spectral profiles, was lost in 5xFAD mice

393   (Fig. 2, B, black line). Thus, the SN-VTA networks [50] in 5xFAD mice seem to be tuned to

394   enhanced synchronization of the neuronal firing activity in the DA-producing nuclei. This is

395   supposedly associated with the mechanisms, which are involved in the compensatory processes

396   initiated by neuronal deficit in SN and VTA [51].

397   *In 5xFAD mice*, a significant attenuation of the spectral differences in EEG from DA nuclei and

398   MC was observed throughout the analyzed frequency range (Fig. 3, C, D). Thus, the functional

399   disturbances in 5xFAD mice seem to be predominantly associated with the attenuation of the

400   oscillatory activity in their DA nuclei-forebrain networks.

401   *Apomorphine effects*

402   In control mice, APO produced a "desynchronising" effect in EEG from MC and HPC, with both

403   attenuated *delta* and enhanced *beta* activities (Fig. 4, A - D, grey lines) similar to those observed

404   in rats treated with APO at the same dose of 1.0 mg/kg [52]. At the lower dose of 0.01 mg/kg,

405   APO has been shown to evoke EEG slowing biased to the *delta* range [38]. At high doses, APO

406   activates postsynaptic DA receptors in terminal areas as DA release in the forebrain is completely

407   blocked by APO at the level of the DA-producing nuclei through the activated autoreceptors [53].

408   Hence, a significant elevation of both suppression in *delta* band and activation in *beta* band in

409   cortical and hippocampal EEG observed in 5xFAD mice (Fig. 4, A - D, black lines) might be

410   explained by the increase in postsynaptic efficacy and/or enhanced sensitivity of DA receptors.

411   Indeed, the neuronal population shrinkage in VTA and SN in 5xFAD mice (Fig. 6, A and C) is

412   expected to result in chronic depletion of DA in the terminal areas of MC and HPC that in turn to

413   initiate compensatory supersensitization of the postsynaptic DA receptors [54]. Similar APO

414   effects in *delta* range of EEG from VTA and SN in mice from both groups (Fig. 4, E and G)

415   underline a relatively high functional stability of basic mechanisms involved in tonic neuronal firing

416   in these nuclei. On the other hand, significant differences revealed in *beta* ("bursting") range in

417   VTA and SN between 5xFAD and nTg mice (Fig. 4, F and H) seem to be associated with the

418   feed-back effects of the APO-activated forebrain on the DA-producing neurons in an attempt to

419   compensate for their APO-suppressed bursting activity [45].

420   APO effects on the EEG spectra in mice from different groups are expressed in both frequency

421   and brain area specific manner (Fig. 5) that might be associated with differences in regional

422   sensitivity of DA receptors to APO. Indeed, *delta* activity, slightly suppressed by APO in MC of

423   mice from both groups (Fig. 5, A, B, grey lines), is roughly affected by APO in VTA, while at lower

424   extent in 5xFAD mice (Fig. 5, A, B, black lines). In contrast, APO enhancing of cortical *beta*

425   activity, comparable in mice from both groups (Fig. 5, C, D, grey lines), is accompanied by a

426   significant *beta* suppression in VTA, predominantly in 5xFAD mice (Fig. 5, C, D, black lines).

427   Given the deficit of DA-producing neurones in 5xFAD mice (Fig. 6, A, C) these results might be

428   concluded to be consistent with the suggestion that DA-ergic deprivation is accompanied by

429   hypersensitization of post- and pre-synaptic DA receptors [54, 55]. Furthermore, the significant

430   *amplification* of APO-induced *delta* activity in EEG from VTA in 5xFAD mice (c.f. Fig. 5, A and B,

431   black lines) is seemingly associated with sensitization of post-synaptic receptors whereas the

432   *beta attenuation* (c.f. Fig. 5, C and D, black lines) may be due to the pre-synaptic modifications.

433   The differences revealed in APO effects on EEG from VTA in 5xFAD and nTg mice and

434   similarities of those in MC (Fig. 5) might be explained by a regional selectivity of DA clearing

435   mechanisms associated with predominant activity of either DAT or catechol-o-methyltransferase

436   (in MC, in particular) [56]. Characteristic DAT levels in MC and DG, different in nTg mice and

437   similar in Tg mice (Fig. 6, D), are indirectly consistent with this suggestion. DAT activity deficit is

438   expected could be accompanied by an increase of DA level in the synaptic clefts that in turn

439   might initiate a compensatory desensitization of both pre- and post-synaptic DA receptors [48].

440   Thus, the deficit of both DA-producing neurones and DAT in 5xFAD mice might be suggested to

441   affect the DA receptors sensitivity resulting in compensatory reorganization of the neuronal

442   networks in/within various brain areas. This is expected could lead to modifications of the APO

443   effects on the EEG oscillations generated by the affected networks.

444   In conclusion, the links between EEG spectra modifications and various intracerebral network

445   transformations in the transgenic model of familial AD, 5xFAD mice, are analyzed in this work.

446   We have shown that EEGs from dopamine-containing areas in the midbrain and in their terminal

447   forebrain structures are altered in these animals. Associations of these alterations with shrinkage

448   of DA-producing cell population, lowered dopamine transporter level, and modified sensitivity of

449   dopamine receptors, which were revealed in this study, are discussed. We suggest that this EEG

450   approach might be a useful tool for further studies of the adaptive/compensatory neuronal

451   network remodelling associated with disturbances in the dopaminergic system. Regardless of the

452   sources of these disturbances, in particular, associated with α-synuclein involvement [57], they

453   are expected to shift the balance between neurogenesis [58] and senescence [59] towards the

454   later, resulting in the neurodegenerative pathology.

457   **Conflict of interest:** The authors declare that they have no conflict of interest.

458

References

[1] Hampel H, Mitchell A, Blennow K, Frank RA, Brettschneider S, Weller L, Moller HJ (2004) Core biological marker candidates of Alzheimer's disease - perspectives for diagnosis, prediction of outcome and reflection of biological activity. *J Neural Transm* **111**(3), 247-272.

[2] Selkoe DJ (2002) Alzheimer's disease is a synaptic failure. *Science* **298**(5594), 789-791.

[3] Vorobyov V, Sengpiel F (2008) Apomorphine-induced differences in cortical and striatal EEG and their glutamatergic mediation in 6-hydroxydopamine-treated rats. *Exp Brain Res* **191**, 277-287.

[4] Oswal A, Brown P, Litvak V (2013) Synchronized neural oscillations and the pathophysiology of Parkinson's disease. *Curr Opin Neurol* **26**, 662-670.

[5] Tampellini D (2015) Synaptic activity and Alzheimer's disease: a critical update. *Front Neurosci* **9**, 423. doi: 10.3389/fnins.2015.00423. eCollection 2015.

[6] Nimmrich V, Draguhn A, Axmacher N (2015) Neuronal Network Oscillations in Neurodegenerative Diseases. *Neuromolecular Med* **17**(3), 270-284.

[7] Palop JJ, Mucke L (2016) Network abnormalities and interneuron dysfunction in Alzheimer disease. *Nat Rev Neurosci* **17**(12), 777-792.

[8] Buzsáki G, Anastassiou CA, Koch C (2012) The origin of extracellular fields and currents--EEG, ECoG, LFP and spikes. *Nat Rev Neurosci* **13**(6), 407-420.

[9] Koenig T, Prichep L, Dierks T, Hubl D, Wahlund LO, John ER, Jelic V (2005) Decreased EEG synchronization in Alzheimer's disease and mild cognitive impairment. *Neurobiol Aging* **26**(2), 165-171.

[10] Lakmache Y, Lassonde M, Gauthier S, Frigon JY, Lepore F (1998) Interhemispheric disconnection syndrome in Alzheimer's disease. *Proc Natl Acad Sci USA* **95**(15), 9042-9046.

[11] Davidson RJ (2004) What does the prefrontal cortex "do" in affect: perspectives on frontal EEG asymmetry research. *Biol Psychol* **67**(1-2), 219-233.

[12] Vorobyov V, Kaptsov V, Gordon R, Makarova E, Podolski I, Sengpiel F (2015) Neuroprotective effects of hydrated fullerene C60: cortical and hippocampal EEG interplay in an amyloid-infused rat model of Alzheimer's disease. *J Alzheimer's Dis* **45**, 217-233.

[13] Wang J, Ikonen S, Gurevicius K, van Groen T, Tanila H (2002) Alteration of cortical EEG in mice carrying mutated human APP transgene. *Brain Res* **943**(2), 181-190.

[14] Cissé M, Sanchez PE, Kim DH, Ho K, Yu GQ, Mucke L (2011) Ablation of cellular prion protein does not ameliorate abnormal neural network activity or cognitive dysfunction in the J20 line of human amyloid precursor protein transgenic mice. *J Neurosci* **31**(29), 10427-10431.

[15] Scott L, Kiss T, Kawabe TT, Hajós M (2016) Neuronal network activity in the hippocampus of tau transgenic (Tg4510) mice. *Neurobiol Aging* **37**, 66-73.

494 [16] Goutagny R, Gu N, Cavanagh C, Jackson J, Chabot JG, Quirion R, Krantic S, Williams S

495 (2013) Alterations in hippocampal network oscillations and *theta-gamma* coupling arise before Aβ

496 overproduction in a mouse model of Alzheimer's disease. *Eur J Neurosci* **37**(12), 1896-1902.

497 [17] Schneider F, Baldauf K, Wetzel W, Reymann KG (2014) Behavioral and EEG changes in

498 male 5xFAD mice. *Physiol Behav* **135**, 25-33.

499 [18] Siwek ME, Müller R, Henseler C, Trog A, Lundt A, Wormuth C, Broich K, Ehninger D,

500 Weiergräber M, Papazoglou A (2015) Altered *theta* oscillations and aberrant cortical excitatory

501 activity in the 5XFAD model of Alzheimer's disease. *Neural Plast* **781731**. doi:

502 10.1155/2015/781731.

503 [19] Scott L, Feng J, Kiss T, Needle E, Atchison K, Kawabe TT, Milici AJ, Hajós-Korcsok E,

504 Riddell D, Hajós M (2012) Age-dependent disruption in hippocampal θ oscillation in amyloid-β

505 overproducing transgenic mice. *Neurobiol Aging* **33**(7), 1481.e13-23, doi:

506 10.1016/j.neurobiolaging.2011.12.010.

507 [20] Crouzin N, Baranger K, Cavalier M, Marchalant Y, Cohen-Solal C, Roman FS,

508 Khrestchatisky M, Rivera S, Féron F, Vignes M (2013) Area-specific alterations of synaptic

509 plasticity in the 5XFAD mouse model of Alzheimer's disease: dissociation between

510 somatosensory cortex and hippocampus. *PLoS One* **8**(9), e74667. doi:

511 10.1371/journal.pone.0074667. eCollection 2013.

512 [21] Oakley H, Cole SL, Logan S, Maus E, Shao P, Craft J, Guillozet-Bongaarts A, Ohno M,

513 Disterhoft J, Van Eldik L, Berry R, Vassar R (2006) Intraneuronal β-amyloid aggregates,

514 neurodegeneration, and neuron loss in transgenic mice with five familial Alzheimer's disease

515 mutations: potential factors in amyloid plaque formation. *J Neurosci* **26**(40), 10129–10140.

516 [22] Marsh SE, Blurton-Jones M (2012) Examining the mechanisms that link β-amyloid and α-

517 synuclein pathologies. *Alzheimers Res Ther* **4**(2), 11. doi: 10.1186/alzrt109. eCollection 2012.

518 [23] Jawhar S, Trawicka A, Jenneckens C, Bayer TA, Wirths O (2012) Motor deficits, neuron loss,

519 and reduced anxiety coinciding with axonal degeneration and intraneuronal Aβ aggregation in the

520 5XFAD mouse model of Alzheimer's disease. *Neurobiol Aging* **33**(1), 196.e29-40 doi:

521 10.1016/j.neurobiolaging.2010.05.027.

522 [24] Buskila Y1, Crowe SE, Ellis-Davies GC (2013) Synaptic deficits in layer 5 neurons precede

523 overt structural decay in 5xFAD mice. *Neuroscience* **254,**152-159.

524 [25] Rubio SE, Vega-Flores G, Martínez A, Bosch C, Pérez-Mediavilla A, del Río J, Gruart A,

525 Delgado-García JM, Soriano E, Pascual M (2012) Accelerated aging of the GABAergic

526 septohippocampal pathway and decreased hippocampal rhythms in a mouse model of

527 Alzheimer's disease. *FASEB J* **26**(11), 4458-4467.

528 [26] Paesler K, Xie K, Hettich MM, Siwek ME, Ryan DP, Schröder S, Papazoglou A, Broich K,

529 Müller R, Trog A, Garthe A, Kempermann G, Weiergräber M, Ehninger D (2015) Limited effects

530   of an eIF2αS51A allele on neurological impairments in the 5xFAD mouse model of Alzheimer's

531   disease. *Neural Plast* **825157**, doi: 10.1155/2015/825157.

532   [27] Dringenberg HC (2000) Alzheimer's disease: more than a 'cholinergic disorder' - evidence

533   that cholinergic-monoaminergic interactions contribute to EEG slowing and dementia. *Behav*

534   *Brain Res* **115**(2), 235-249.

535   [28] Koch G, Esposito Z, Codecà C, Mori F, Kusayanagi H, Monteleone F, Di Lorenzo F, Bernardi

536   G, Martorana A (2011) Altered dopamine modulation of LTD-like plasticity in Alzheimer's disease

537   patients. *Clin Neurophysiol* **122**(4), 703-707.

538   [29] Himeno E, Ohyagi Y, Ma L, Nakamura N, Miyoshi K, Sakae N, Motomura K, Soejima N,

539   Yamasaki R, Hashimoto T, Tabira T, LaFerla FM, Kira J (2011) Apomorphine treatment in

540   Alzheimer mice promoting amyloid-β degradation. *Ann Neurol* **69**(2), 248-256.

541   [30] Lu J, Li X, Wang Q, Pei G (2017) Dopamine D2 receptor and β-arrestin 2 mediate Amyloid-β

542   elevation induced by anti-parkinson's disease drugs, levodopa and piribedil, in neuronal cells.

543   *PLoS One* **12**(3), e0173240. doi: 10.1371/journal.pone.0173240.

544   [31] Rosen GD, Williams AG, Capra JA, Connolly MT, Cruz B, Lu L, Airey DC, Kulkarni K,

545   Williams RW (2000) The Mouse Brain Library @ www.mbl.org. Int Mouse Genome Conference

546   14: 166. www.mbl.org.

547   [32] Bussière T, Bard F, Barbour R, Grajeda H, Guido T, Khan K, Schenk D, Games D, Seubert

548   P, Buttini M (2004) Morphological characterization of Thioflavin-S-positive amyloid plaques in

549   transgenic Alzheimer mice and effect of passive A*beta* immunotherapy on their clearance. *Am J*

550   *Pathol* **165**(3), 987-995.

551   [33] Franklin KBJ, Paxinos G (2007) The Mouse Brain in Stereotaxic Coordinates. Third edition

552   Academic Press, New York, USA.

553   [34] Gerfen CR (2003) Basic Neuroanatomical Methods. *Current Protocols in Neuroscience*

554   00:1.1:1.1.1–1.1.11. doi: 10.1002/0471142301.ns0101s23, John Wiley & Sons.

555   [35] Gal'chenko AA, Vorobyov VV (1999) Analysis of electroencephalograms using a modified

556   amplitude-interval algorithm. *Neurosci Behav Physiol* **29**, 157-160.

557   [36] Hökfelt T, Martensson R, Björklund A, Kheinau S, Goldstein M (1984) In Björklund A, Hökfelt

558   T. (Eds*.), Handbook of Chemical Neuroanatomy*. Elsevier Science B.V, Amsterdam, Part 1, Vol.

559   2, pp. 277-379.

560   [37] Sotnikova TD, Beaulieu JM, Gainetdinov RR, Caron MG (2006) Molecular biology,

561   pharmacology and functional role of the plasma membrane dopamine transporter. *CNS Neurol*

562   *Disord Drug Targets* **5**, 45–56.

563   [38] Sebban C, Zhang XQ, Tesolin-Decros B, Millan MJ, Spedding M (1999) Changes in EEG

564   spectral power in the prefrontal cortex of conscious rats elicited by drugs interacting with

565   dopaminergic and noradrenergic transmission. *Br J Pharmacol* **128**(5), 1045-1054.

566   [39] Vyazovskiy VV, Achermann P, Borbély AA, Tobler I (2004) The dynamics of spindles and

567   EEG slow-wave activity in NREM sleep in mice. *Arch Ital Biol* **142**(4), 511-523.

568   [40] Mucke L, Selkoe DJ (2012) Neurotoxicity of amyloid β-protein: synaptic and network

569   dysfunction. Cold Spring Harb. *Perspect Med* **2**(7), a006338. doi: 10.1101/cshperspect.a006338.

570   [41] Paladini CA, Roeper J (2014) Generating bursts (and pauses) in the dopamine midbrain

571   neurons. *Neuroscience* **282**, 109-121.

572   [42] Hage TA, Khaliq ZM (2015) Tonic firing rate controls dendritic Ca2+ signaling and synaptic

573   gain in substantia nigra dopamine neurons. *J Neurosci* **35**(14), 5823-5836.

574   [43] Seeger-Armbruster S, von Ameln-Mayerhofer A (2013) Short- and long-term unilateral 6-

575   hydroxydopamine lesions in rats show different changes in characteristics of spontaneous firing

576   of substantia nigra pars reticulata neurons. *Exp Brain Res* **224**(1), 15-24.

577   [44] Duda J, Pötschke C, Liss B (2016) Converging roles of ion channels, calcium, metabolic

578   stress, and activity pattern of Substantia nigra dopaminergic neurons in health and Parkinson's

579   disease. *J Neurochem* **139** Suppl 1, 156-178.

580   [45] Tong ZY, Overton PG, Clark D (1996) Antagonism of NMDA receptors but not AMPA/kainate

581   receptors blocks bursting in dopaminergic neurons induced by electrical stimulation of the

582   prefrontal cortex. *J Neural Transm* **103**, 889–904.

583   [46] Au-Young SM, Shen H, Yang CR (1999) Medial prefrontal cortical output neurons to the

584   ventral tegmental area (VTA) and their responses to burst-patterned stimulation of the VTA:

585   neuroanatomical and in vivo electrophysiological analyses. *Synapse* **34**(4), 245-255.

586   [47] Sesack SR, Grace AA (2010) Cortico-basal ganglia reward network: microcircuitry.

587   *Neuropsychopharmacology* **35**, 27-47.

588   [48] Lohr KM, Masoud ST, Salahpour A, Miller GW (2017) Membrane transporters as mediators

589   of synaptic dopamine dynamics: implications for disease. *Eur J Neurosci* **45**(1), 20-33.

590   [49] Benchenane K, Peyrache A, Khamassi M, Tierney PL, Gioanni Y, Battaglia FP, Wiener SI

591   (2010) Coherent *theta* oscillations and reorganization of spike timing in the hippocampal -

592   prefrontal network upon learning. *Neuron* **66**(6), 921-936.

593   [50] Ferreira JG, Del-Fava F, Hasue R.H, Shammah-Lagnado SJ (2008) Organization of ventral

594   tegmental area projections to the ventral tegmental area-nigral complex in the rat. *Neuroscience*

595   **153**(1), 196-213.

596   [51] Golden JP, Demaro JA 3rd, Knoten A, Hoshi M, Pehek E, Johnson EM Jr, Gereau RW 4th,

597   Jain S (2013) Dopamine-dependent compensation maintains motor behavior in mice with

598   developmental ablation of dopaminergic neurons. *J Neurosci* **33**(43), 17095-17107.

599   [52] Gessa GL, Porceddu ML, Collu M, Mereu G, Serra M, Ongini E, Biggio G (1985) Sedation

600   and sleep induced by high doses of apomorphine after blockade of D-1 receptors by SCH 23390.

601   *Eur J Pharmacol* **109**(2), 269-274.

602   [53] Zetterström T, Ungerstedt U (1984) Effects of apomorphine on the in vivo release of

603   dopamine and its metabolites, studied by brain dialysis. *Eur J Pharmacol* **97**(1-2), 29-36.

604   [54] Kostrzewa RM, Kostrzewa JP, Brown RW, Nowak P, Brus R (2008) Dopamine receptor

605   supersensitivity: development, mechanisms, presentation, and clinical applicability. *Neurotox Res*

606   **14**, 121–128.

607   [55] Robinson S, Smith DM, Mizumori SJ, Palmiter RD (2004) Firing properties of dopamine

608   neurons in freely moving dopamine-deficient mice: effects of dopamine receptor activation and

609   anesthesia. *Proc Natl Acad Sci USA* **101**(36), 13329-13334.

610   [56] Cockerham R, Liu S, Cachope R, Kiyokage E, Cheer JF, Shipley MT, Puche AC (2016)

611   Subsecond Regulation of Synaptically Released Dopamine by COMT in the Olfactory Bulb. *J

612   Neurosci* **36**(29), 7779-7785.

613   [57] Garcia-Reitboeck P, Anichtchik O, Dalley JW, Ninkina N, Tofaris GK, Buchman VL,

614   Spillantini MG (2013) Endogenous *alpha*-synuclein influences the number of dopaminergic

615   neurons in mouse substantia nigra. *Exp Neurol* **248**, 541-545.

616   [58] Höglinger GU, Rizk P, Muriel MP, Duyckaerts C, Oertel WH, Caille I, Hirsch EC (2004)

617   Dopamine depletion impairs precursor cell proliferation in Parkinson disease. *Nat Neurosci* 7(7),

618   726-735.

619   [59] Nekrasov PV, Vorobyov VV (2018) Dopaminergic mediation in the brain aging and

620   neurodegenerative diseases: a role of senescent cells. *Neural Regen Res* 13(4), 649-650.

621

Figures legends

623 **Figure 1.** Typical patterns in 12-s fragments of baseline EEG in wakeful and behaviourally active

624 non-transgenic (nTg) and 5xFAD (Tg) mice (**A** and **B**, respectively) and their frequency spectra

625 (**C** - **F**) in the secondary motor cortex (MC), hippocampus (HPC), and the nuclei containing DA-

626 synthesizing neurons: substantia nigra (SN) and ventral tegmental area (VTA).

627 On **A** and **B,** time calibration is 1 sec, amplitude calibration is 100 μV. On **C** - **F**, abscissa is a

628 frequency subband marked with its mean value, in hertz; ordinate is summed amplitudes of EEG

629 in each of 20 subbands, normalized to a sum of all amplitude values, in arbitrary units. Alternating

630 white and grey bars indicate "classical" EEG frequency bands (from left to right): *delta*, *theta*,

631 *alpha*, and *beta*.

632

633 **Figure 2.** Averaged amplitude-frequency spectra of 12-s baseline EEG fragments recorded from

634 MC (**A**), HPC (**B**), VTA (**C**), and SN (**D**) for 60 min in non-transgenic (nTg, n = 9) and 5xFAD (Tg,

635 n = 6) mice (dashed and solid lines, respectively) and spectral ratios (narrow grey bars) between

636 the groups (Tg/nTg).

637 Abscissa is a frequency subband marked with its mean value, in hertz; the left ordinate is

638 summed absolute values of EEG amplitudes in each of 20 subbands, normalized to sum of all

639 amplitude values, in arbitrary units; the right ordinate is a ratio of the EEG amplitudes, calculated

640 as (Tg - nTg) / nTg, in %. Vertical lines are ±1SEM; diamond denotes a significant difference

641 between the groups (p<0.05, Wilcoxon test). Alternating white and grey bars indicate "classical"

642 EEG frequency bands (from left to right): *delta*, *theta*, *alpha*, and *beta*.

643

644 **Figure 3.** Relations between averaged amplitude-frequency spectra of 12-s baseline EEG

645 fragments recorded from the secondary motor cortex (MC), superficial layers of the

646 hippocampal CA1 area (HPC), substantia nigra (SN), and ventral tegmental area (VTA) for

647 60 min in non-transgenic (nTg, n = 9) and 5xFAD (Tg, n = 6) mice (dashed and solid lines,

648 respectively). Abscissa is a frequency subband marked with its mean value in hertz; ordinate

649 is a ratio of summed absolute values of baseline EEG amplitudes in each of 20 subbands,

650 normalized to sum of all amplitudes of EEG recorded from different brain areas, calculated

651 as (Area 1 - Area 2) / Area 2, in %, characterizing genetically determined EEG relations

652 between them. Vertical lines are ±1SEM; diamond denotes a significant difference between

653 the groups (p<0.05, Wilcoxon test). Alternating white and grey bars indicate "classical" EEG

654 frequency bands (from left to right): *delta*, *theta*, *alpha*, and *beta*.

655

656 **Figure 4.** Evolution of apomorphine (APO, 1.0 mg/kg, s.c.) *vs.* saline effects in *delta* and *beta*

657 frequency bands (**A**, **C**, **E**, **G** and **B**, **D**, **F**, **H**, respectively) of EEG from MC, HPC, VTA, and SN in

658 non-transgenic (nTg, n = 9) and 5xFAD (Tg, n = 6) mice (gray and black lines, respectively).

659 Abscissa shows time after injection, marked in 10-min intervals. Ordinate is a ratio of the

660 averaged EEG amplitudes in the indicated frequency bands, obtained in experiments with saline

661 and APO in each group, and estimated as (APO - Saline) / Saline, in %, characterizing APO

662 effects in nTg and Tg groups. A difference between baseline EEG ratios in Tg and nTg mice was

663 used for normalization of APO effects in Tg group. Diamond denotes a significant difference

664 between the groups ($p < 0.05$, Wilcoxon test). Error bars show ±1 SEM.

665

666 **Figure 5.** Evolution of apomorphine (APO, 1.0 mg/kg, s.c.) effects in *delta* and *beta* bands of

667 EEG from MC and VTA in non-transgenic (nTg) and 5xFAD mice (n = 9 and 6, respectively).

668 Abscissa shows time after APO injection, marked in 10-min intervals. Ordinate is EEG amplitudes

669 (in arbitrary units) summed in the indicated frequency bands in different brain areas separately for

670 each group and normalized to EEG baseline values in MC (horizontal dashed lines). Diamond

671 denotes a significant difference between the groups ($p < 0.05$, Wilcoxon test). Error bars show ±1

672 SEM.

673

674 **Figure 6.** Distribution of tyrosine hydroxylase immunopositive (TH+) cells (**A, C**) and dopamine

675 transporter (DAT) (**B, D**) in different brain areas in non-transgenic (nTg) and transgenic (Tg,

676 5xFAD) mice. On **A,** photomicrographs from nTg (**a**, **b**) and Tg (**c**, **d**) experimental mice display

677 TH+ cells (black pyramids) in the ventral tegmental area (VTA) and the substantia nigra (SN),

678 outlined by dashed ellipsis on the centered section, modified from [31]. On **B**, photomicrographs

679 display DAT vesicles distributions (black spots) in the dentate gyrus (DG) from nTg (**a**) and Tg (**b**)

680 experimental mice in the area outlined by open white rectangle. Obvious loss of TH-positive

681 neurons and DAT vesicles is observed in 5xFAD mice. Horizontal white bars on **A** and **B** denote

682 the scales of 50 µm. On **C,** abscissa demonstrates the brain areas with DA-producing neurons,

683 VTA and SN; on **D**, abscissa shows the brain areas containing DAT: MC, DG, and hippocampal

684 CA1-CA2, and CA3-CA4 fields. Ordinate on **C** is the number of TH-positive cells in the

685 boundaries of VTA and SN; ordinate on **D** is the DAT-containing area (in mm^2), accounted in the

686 frame of 0.55 mm x 0.45 mm (0.25 mm^2). Stars denote significant differences between Tg and

687 nTg groups, ** – $p < 0.01$, *** – $p < 0.001$ (two-tailed U-test).

688

Baseline EEG fragments and their frequency spectra
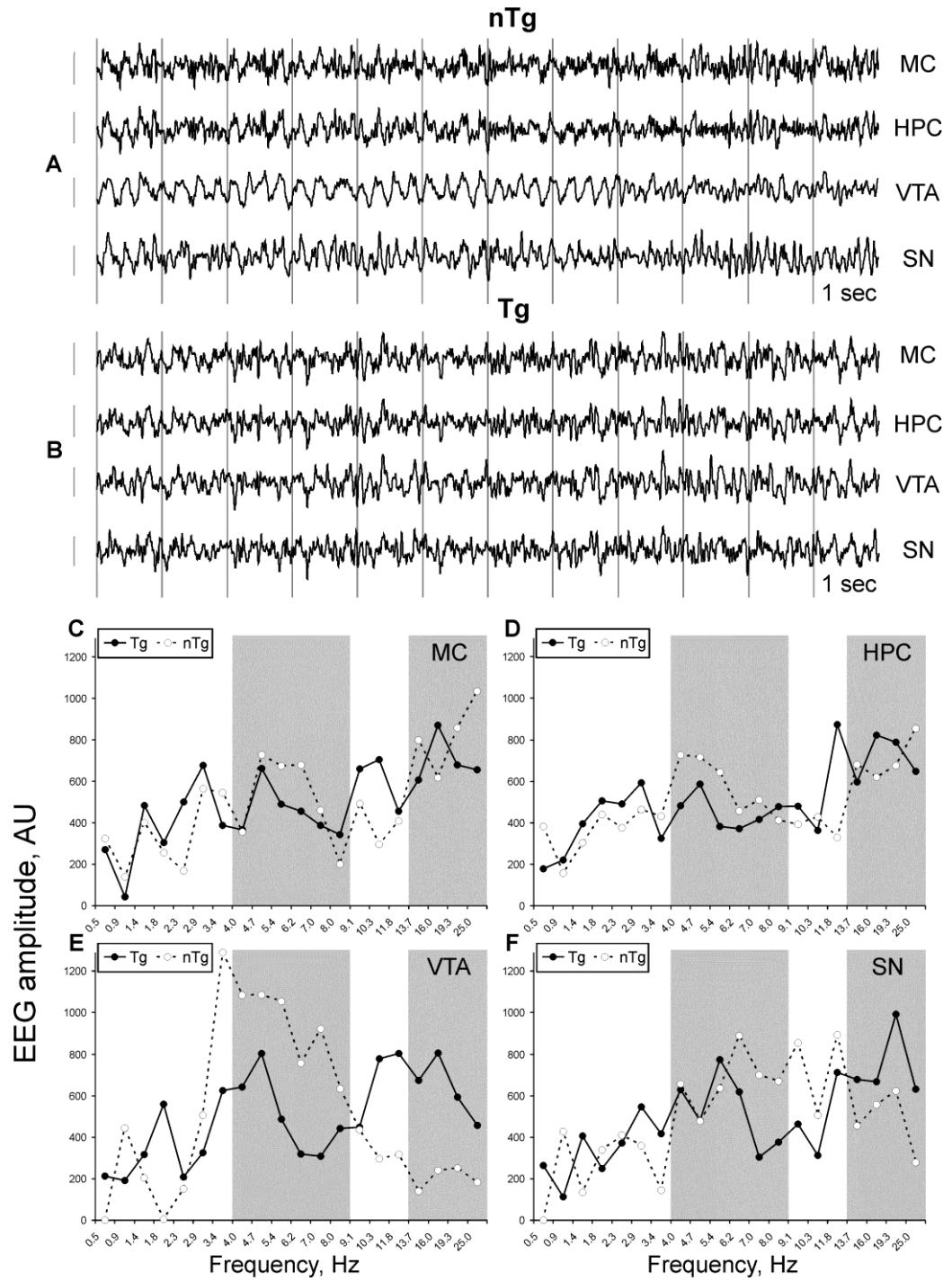
Figure 1

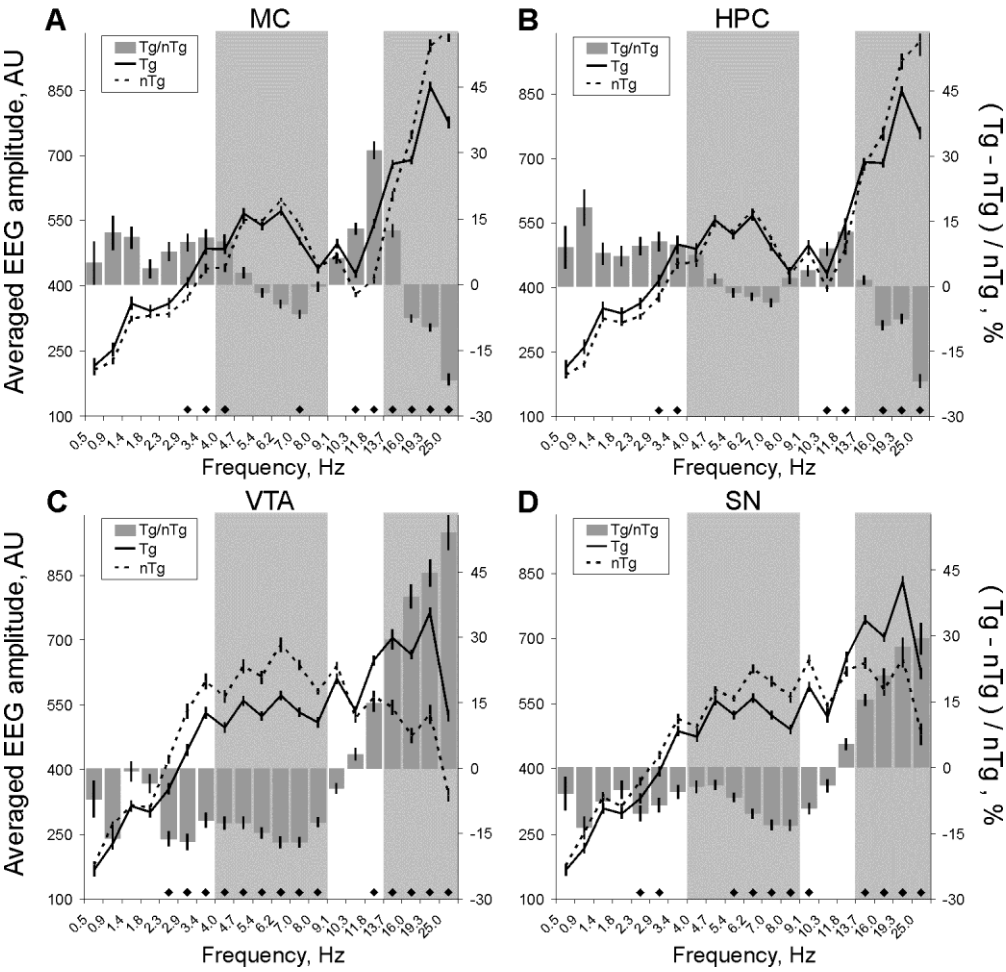Averaged baseline EEG spectra in 5xFAD *vs.* non-transgenic mice

Figure 2

692
693
694

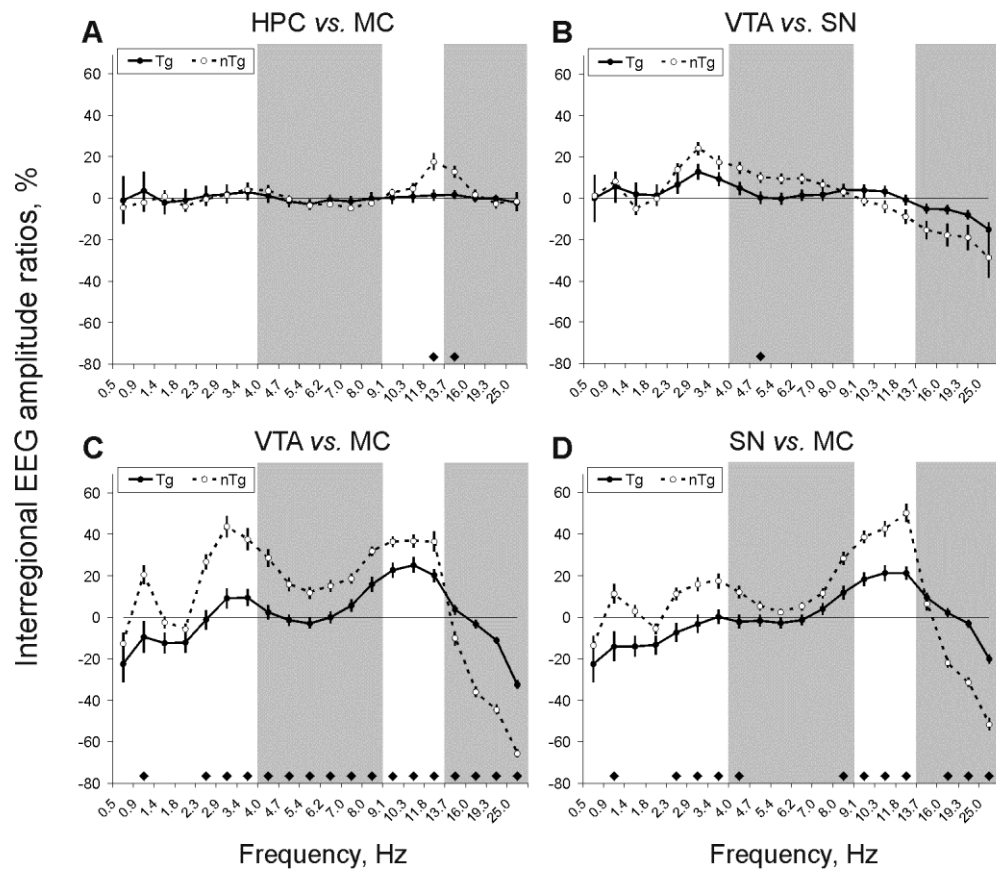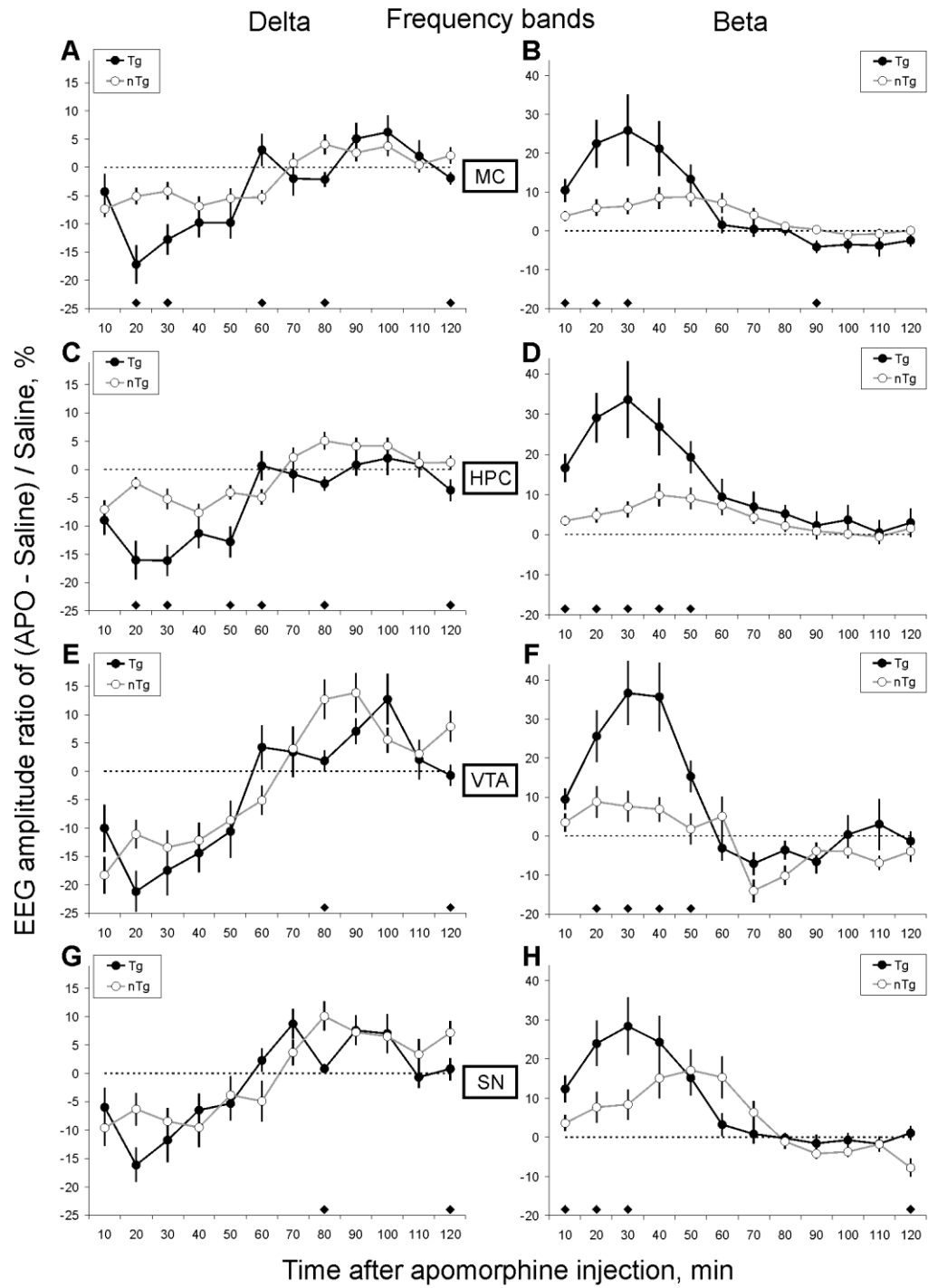Baseline EEG relations between the brain areas in mice from different groups

Figure 3

EEG effects of APO *vs*. saline in 5xFAD and control mice

Figure 4
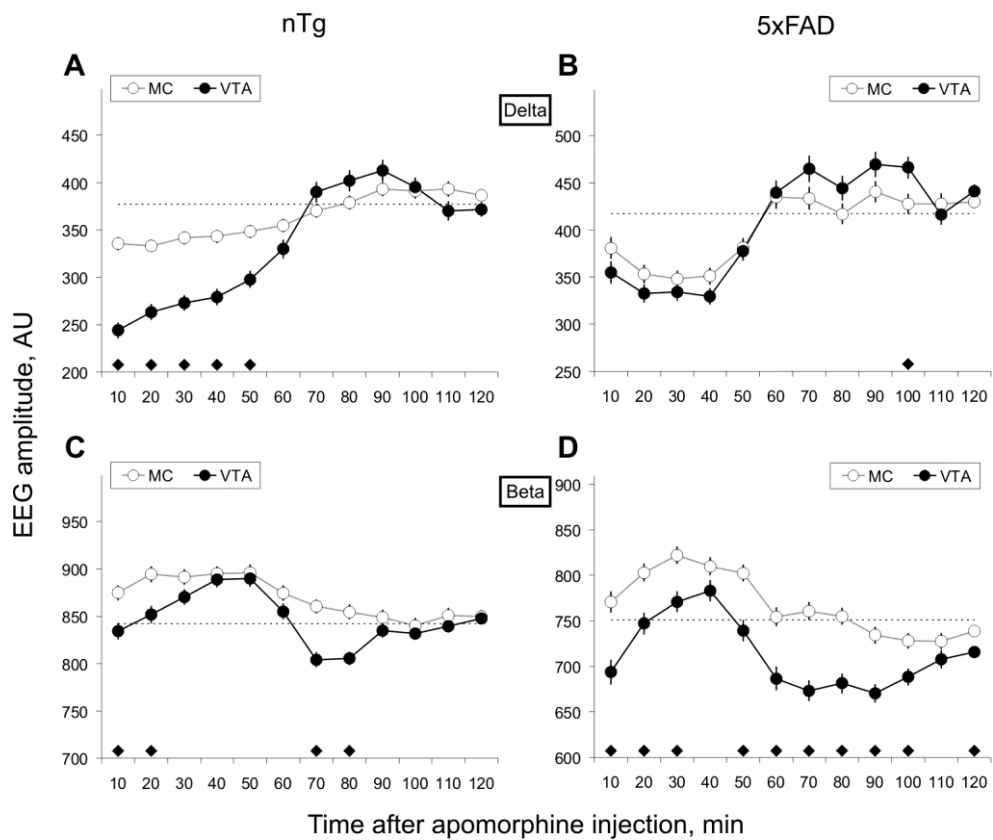
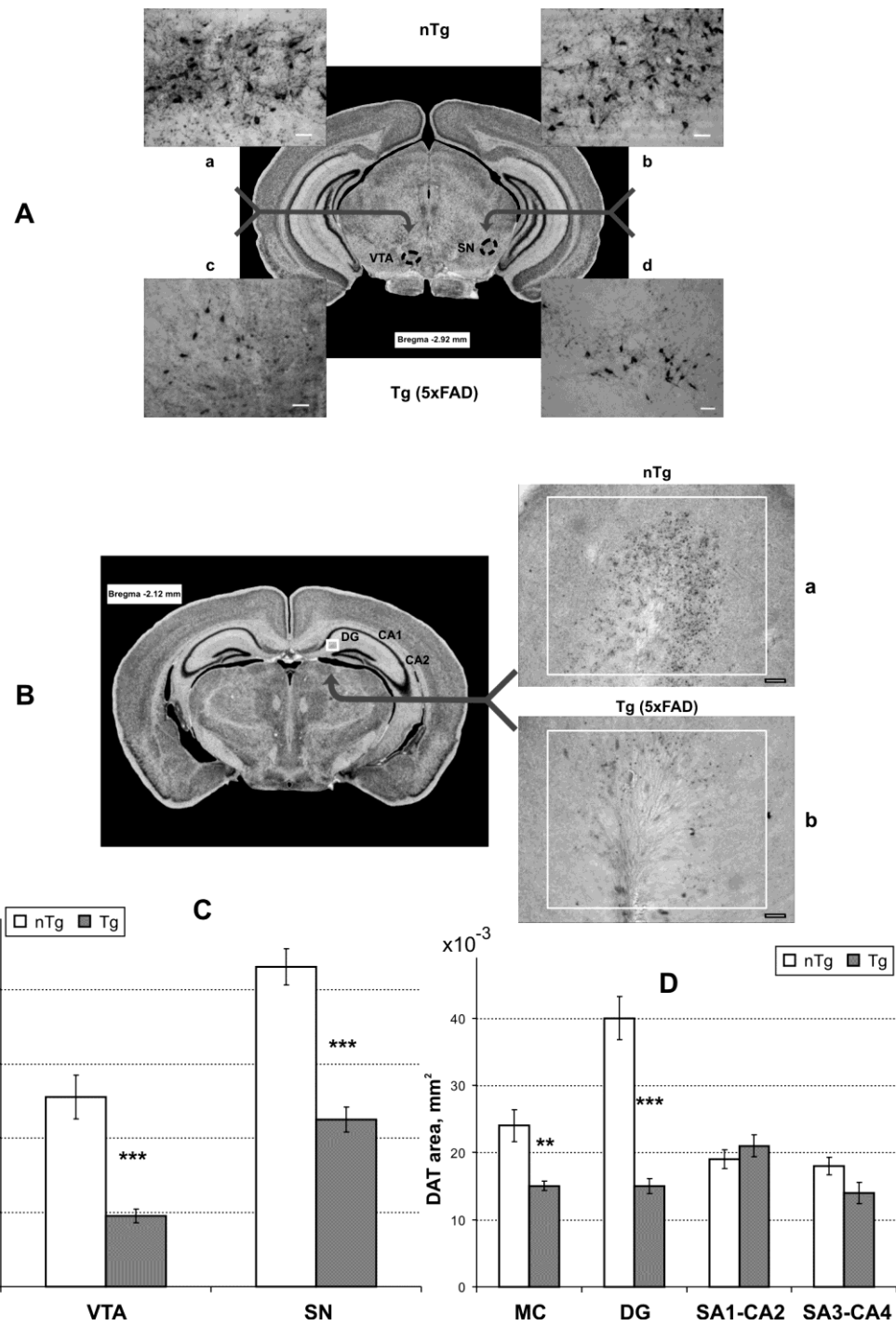APO effects in EEG from MC and VTA in mice from different groups

701
702 **Figure 5**
703

nTg

A

a   b

VTA   SN

c   d

Bregma -2.92 mm

Tg (5xFAD)

Bregma -2.12 mm

DG   CA1

CA2

B

nTg

a

Tg (5xFAD)

b

C

The number of TH+ cells within the area

□ nTg ▨ Tg

***

***

VTA   SN

D

x10⁻³

□ nTg ▨ Tg

DAT area, mm²

**

***

MC   DG   SA1-CA2 SA3-CA4

704
705   **Figure 6**

27